Chemical Science

ROYAL SOCIETY OF CHEMISTRY

EDGE ARTICLE

View Article Online
View Journal | View Issue

Cite this: *Chem. Sci.*, 2025, **16**, 7579

All publication charges for this article have been paid for by the Royal Society of Chemistry

Received 4th February 2025
Accepted 24th March 2025

DOI: 10.1039/d5sc00899a

rsc.li/chemical-science

The role of structural defects in the fluoride-mediated synthesis of aluminosilicate zeolites†

Kingsley Christian Kemp,[a] Ömer F. Altundal,[b] Donghui Jo,[c] Weidong Huang,[de] Qiang Wang,[de] Feng Deng,[de] German Sastre *[b] and Suk Bong Hong *[a]

The existence of framework defects in zeolites, an important class of industrial catalysts and adsorbents, has long been recognized, but little is known about their exact role in zeolite crystallization. Here we show that despite their relatively high framework Al content (Si/Al = 11.5–13.8), as-synthesized PWO, PWW and RTH zeolites, obtained using various trimethylpyridinium cation isomers as organic structure-directing agents (OSDAs) in concentrated fluoride media, contain unexpectedly large amounts of $SiO^{-}\cdots HOSi$ defects which counterbalance the charge of 11–39% of the total OSDA cations occluded per unit cell, but have only a negligible amount (<0.1 ions per unit cell) of fluoride anions. The results suggest that the phase selectivity of the crystallization in the presence of fluoride ions may be determined by a combination of Al incorporation into the silicate framework, the type of OSDAs used and the microstructure and concentration of $SiO^{-}\cdots HOSi$ defects formed. This study provides a new basis for better understanding the fundamental aspects of zeolite crystallization mechanisms.

Introduction

Zeolites, both natural and synthetic, are microporous crystalline materials that are widely used as commercial catalysts and adsorbents, largely because of their uniformity in pore shape and size. Yet despite this success, there is a need for zeolites with desired pore architectures and physicochemical properties, for example, to develop green technologies for carbon capture and energy conversion.[1,2] However, the current understanding of zeolite crystallization mechanisms is poor so that the rational synthesis of novel zeolite structures and/or compositions remains highly challenging.

None of the crystalline solids can be completely free of internal structural defects, which is also the case for zeolites and zeolite-like materials. In particular, many important properties of high-silica zeolites like their ion exchange capacity, catalytic activity and (hydro)thermal stability have long been recognized to differ according to the concentration and nature of their defects.[3–8] Intrazeolitic defect sites can be broadly categorized as siloxy (SiO^{-}) and silanol (SiOH) groups: the former can balance the positive charge of inorganic structure-directing agents (ISDAs) and organic structure-directing agents (OSDAs) or be involved in intermolecular hydrogen bonding to the SiOH group, whereas the latter is generated by hydrolysis of Si–O–Si linkages, by missing tetrahedral atoms (T-atoms; T = Si, Al, B, *etc.*), or by stacking disorder.[9–12] On the other hand, the formation of discrete nuclei with the structural identity of the crystallizing phase is generally believed to trigger zeolite crystallization.[13] Apparently, zeolite nuclei should be substantially more defective than well-grown zeolite crystals because of their embryonic nature. This led us to consider the possibility that when they are stable enough to survive in the crystallization medium, the microstructure and concentration of their defects, apart from or together with those of ISDAs and/or OSDAs in the synthesis mixture, could be determinant of the phase selectivity during zeolite crystallization. In fact, structural defects have long been reported to be present at early stages of zeolite synthesis.[9] However, little attention has been paid to whether and how they could play a structure-directing role in zeolite nucleation and crystal growth, especially in fluoride media.[14–16]

PST-21 (framework type PWO) and PST-22 (PWW) are two high-silica (Si/Al ~ 10) zeolites that were first synthesized *via* the so-called excess fluoride approach ($HF/OSDA^{q+} \geq 2q$) using

[a]*Center for Ordered Nanoporous Materials Synthesis, Division of Environmental Science and Engineering, POSTECH, Pohang 37673, South Korea. E-mail: sbhong@postech.ac.kr*

[b]*Instituto de Tecnologia Quimica (UPV-CSIC), Universidad Politécnica de Valencia, Avenida Naranjos s/n, Valencia 46022, Spain. E-mail: gsastre@itq.upv.es*

[c]*Low-Carbon Petrochemical Research Center, Korea Research Institute of Chemical Technology, Daejeon 34114, South Korea*

[d]*State Key Laboratory of Magnetic Resonance and Atomic and Molecular Physics, National Center for Magnetic Resonance in Wuhan, Innovation Academy for Precision Measurement Science and Technology, Chinese Academy of Sciences, Wuhan 430071, P. R. China*

[e]*University of Chinese Academy of Sciences, Beijing 100049, P. R. China*

† Electronic supplementary information (ESI) available: OSDA and zeolite preparation, analytical and computational methods, and characterization results. CIF files of all optimized geometries of the zeolite–OSDA systems in Tables S6–S13. CCDC 2366700 (134TMP-PWO) and 2366701 (135TMP-PWW). For ESI and crystallographic data in CIF or other electronic format see DOI: https://doi.org/10.1039/d5sc00899a

1,2,3-trimethylimidazolium (123TMI) and 1,3,4-trimethylimidazolium (134TMI) or 1,2,3,4-tetramethylimidazolium (1234TMI) cations as OSDAs, respectively.[17,18] While the PWO structure consists of two intersecting 9-ring (4.2 × 4.4 Å) channels, the PWW one has intersecting 10-ring (5.2 × 6.0 Å) and 8-ring (3.3 × 3.6 Å) channels. In the present study, we report the fluoride-mediated synthesis of aluminosilicate (Si/Al = 11.5–13.8) zeolites with PWO, PWW and RTH topologies in the presence of various trimethylpyridinium (TMP) cation isomers as OSDAs. RTH is a small-pore zeolite containing 22-hedral ($[4^6 5^8 6^4 8^4]$) *t-rth* cages, unlike PWO and PWW.[19] Up to now, many alkylpyridinium-based SDAs have been used in the synthesis of a number of zeolites with different framework structures (*e.g.* ZSM-22 (TON), ferrierite (FER), ITQ-12 (ITW), RUB-13 (RTH), SCM-14 (SOR), ZSM-5 (MFI), *etc.*) and compositions (aluminosilicate, germanosilicate and pure-silica) in hydroxide or fluoride media.[20–29] However, none of them were reported to direct the synthesis of PWO and PWW. More interestingly, our experimental results demonstrate that considerable (11–39% of the total OSDA cations occluded per unit cell) $SiO^- \cdots HOSi$ defects exist in as-synthesized aluminosilicate PWO, PWW and RTH zeolites, unlike in as-synthesized pure-silica ITQ-12 (ITW) that was crystallized in the presence of any of the TMP cation isomers studied here. To elucidate the origin of this anomaly, we have carried out synthesis energy calculations for various TMP cations in a series of zeolites with different framework structures and anion compositions.[30–32]

Experimental section

Zeolite synthesis

In a typical preparation of a series of TMP cation isomers in their hydroxide form used as OSDAs in zeolite synthesis, a mixture of 0.10 mol of an appropriate dimethylpyridine and 0.3 mol of iodomethane (98%, Kanto) was stirred in 200 mL of acetone at 25 °C for 3 days. Further details can be found in the ESI.† The other reagents included tetraethylorthosilicate (98%, Aldrich), aluminum hydroxide ($Al(OH)_3$, Aldrich), hydrofluoric acid (48%, J.T. Baker) and deionized water. The composition of the final zeolite synthesis mixture was $0.5R \cdot xHF \cdot yAl_2O_3 \cdot 1.0SiO_2 \cdot 5.0H_2O$, where R is OSDA prepared here, x is varied between $0.5 < x < 1.5$ and y is 0 or 0.05. The final synthesis mixture was transferred into a 23 mL Teflon-lined autoclave and heated under rotation (60 rpm) at 160 °C for 14–21 days. Further details can be found in the ESI.† When necessary, as-synthesized zeolites were calcined in air at 600–750 °C for 8 h, depending on their structure type, to remove the occluded organic SDA.

Analytical methods

Powder X-ray diffraction (PXRD), elemental and thermal analyses, scanning electron microscopy (SEM), and ^1H–^{13}C cross polarization (CP), ^1H, ^{19}F, ^{27}Al and ^{29}Si Magic Angle Spinning (MAS) Nuclear Magnetic Resonance (NMR) measurements were performed as described in our previous papers.[17,33] Synchrotron PXRD data for as-synthesized PWO and PWW zeolites were collected on the 2D and 5A beamlines equipped with a ceramic furnace at the Pohang Accelerator Laboratory (PAL; Pohang, Korea) using monochromated X-rays (λ = 0.7000 and 0.6926 Å, respectively). The Rietveld refinements on the occluded OSDAs was performed using the rigid-body method.[34] A summary of experimental and crystallographic data for 134TMP-PWO and 135TMP-PWW are shown in Table S1,† and their atomic coordinates, thermal parameters and selected bond lengths and angles are given in Tables S2–S5.†

^1H double quantum–single quantum (DQ–SQ) MAS and triple quantum–single quantum (TQ–SQ) MAS NMR spectra were recorded on a Bruker Avance III 500 spectrometer and 1.9 mm triple resonance probe. Prior to the NMR experiments, the sample was dried at 200 °C under dynamic vacuum. All experiments were carried out at a spinning frequency of 25 kHz and a $\pi/2$ pulse length of 1.9 μs, using the $R12_2^5$ symmetry-based recoupling scheme[35] ($\tau_{re} \approx 210$ μs) for DQ and the $SR30_4^{10}$ recoupling scheme[36] ($\tau_{re} \approx 632$ μs) for TQ. A total of 512 scans were collected for each of the 64 rotor-synchronized t_1 increments with a recycle delay of 2 s. The spectra are referenced with respect to adamantane at 1.78 ppm.

Synthesis energy calculations

The zeoTsda software[37] contains a suite of programs with the General Utility Lattice Program (GULP)[38] at the heart, whose Monte Carlo and lattice energy minimization algorithms are used to, respectively, include OSDA molecules until the optimum loading is found and optimise their location in the zeolite micropores. The total energies ($E_{zeolite-OSDAF}$) of these structures, for pure-silica composition, were calculated through a single point energy calculation and the so-called synthesis energy (E_{syn}) values obtained using eqn (1), as previously described:[30–32]

$$E_{syn} = E_{zeolite-OSDAF} + 2 \times E_{H_2O} - \frac{q}{m+p} \times E_{OSDAF} - \frac{m+q}{m+p} \times E_{Si(OH)_4} \quad (1)$$

where E_{OSDAF} is the energy of the OSDA neutralized with fluoride anions.

For defect-free aluminosilicate zeolite calculations the starting point was the unit cells for the optimally loaded OSDA pure-silica ones. Here the Si/Al ratio was chosen to either (i) compensate for the entire OSDA charge or (ii) to represent the experimentally obtained one. The zeoTAl software was used to generate random Al distributions for each zeolite–OSDA pair. Of these pairs the lowest energy selection following Lowenstein's rule was optimized and its E_{syn} value was calculated using eqn (2):

$$E_{syn} = E_{zeolite-OSDAF} + 2 \times E_{H_2O} - \frac{(p-q)}{(m+p)} \times (E_{OSDAOH} + E_{Al(OH)_3}) - \frac{q}{m+p} \times E_{OSDAF} - \frac{m+q}{m+p} \times E_{Si(OH)_4} \quad (2)$$

where $E_{\text{zeolite–OSDAF}}$ is the energy of a zeolite–OSDAF pair with a given Si/Al ratio, E_{OSDAOH} the energy of the OSDA neutralized with hydroxide anions, and 'p', 'q', '$p - q$' and '$m + q$' the number of OSDA molecules, fluoride anions, Al and Si atoms, respectively. For pure-silica zeolites, eqn (1) is a particular case of the more general eqn (2) when there is no Al ($p - q = 0$).

The calculation was then expanded to accommodate for aluminosilicate zeolites containing 1SiOH–1SiO$^-$ clusters (1 : 1 connectivity defects) using the same work flow and the E_{syn} calculated using eqn (3a):

$$E_{\text{syn}} = E_{\text{zeolite–OSDAF}} + 2 \times E_{\text{H}_2\text{O}} - \frac{p-q+d}{m+p} \times E_{\text{OSDAOH}} - \frac{(p-q)}{(m+p)} \times E_{\text{Al(OH)}_3} - \frac{q}{m+p} \times E_{\text{OSDAF}} - \frac{m+q}{m+p} \times E_{\text{Si(OH)}_4} \quad (3a)$$

where 'd' is the number of SiO$^-\cdots$HOSi defects, and '$p - q$' and 'q' the numbers of framework Al atoms and F$^-$ ions, respectively. Here, the number of OSDAs is '$p + d$' which leads to the overall zero charge [$(p + d) - \{(p - q) + q + d\}$] in the zeolite structure.

When the defect type in the structure changes to the 3SiOH–1SiO$^-$ cluster model (2 : 1 connectivity defect or 3 : 1 vacancy defect), E_{syn} is defined by the following equation:

$$E_{\text{syn}} = E_{\text{zeolite–OSDAF}} + \frac{2(m+p)-d}{m+p} \times E_{\text{H}_2\text{O}} - \frac{p-q+d}{m+p} \times E_{\text{OSDAOH}} - \frac{(p-q)}{(m+p)} \times E_{\text{Al(OH)}_3} - \frac{m+q}{m+p} \times E_{\text{Si(OH)}_4} \quad (3b)$$

The 1 : 1 connectivity defect, 2 : 1 connectivity defect and 3 : 1 vacancy defect models were employed to generate the initial geometries of defects in as-synthesized 134TMP-PWO, 135TMP-PWW and 123TMP-RTH according to the ^{1}H MAS NMR results (Fig. 3, S7 and S8†). Structures of 134TMP-PWO, 135TMP-PWW and 123TMP-RTH with various defect types were subsequently optimized using DFT calculations to acquire an accurate geometry of defects and O$\cdots$O distances within these defects.

Details regarding the force field, Lennard-Jones, three-body, Morse and Buckingham potential parameters are given in the ESI and Tables S15–S19.† Additionally, force field potential parameters for species unused in this work are presented in Table S20.† This will make it easier for the users to get all parameters for this general and transferable force field.

Results and discussion

Zeolite synthesis

Table 1 lists the representative products from pure-silica (Si/Al = ∞) and aluminosilicate (Si/Al = 10) zeolite syntheses at different HF/OSDA ratios (1.0–3.0) using 1,2,3-trimethylpyridinium (123TMP), 1,2,4-trimethylpyridinium (124TMP), 1,2,5-trimethylpyridinium (125TMP), 1,2,6-trimethylpyridinium (126TMP), 1,3,4-trimethylpyridinium (134TMP), or 1,3,5-trimethylpyridinium (135TMP) ions under rotation (60 rpm) at 160 °C for 14 days. Here we selected these six TMP isomers as OSDAs because their positive charge is localized on the N atom, unlike in the TMI cations where the charge is spread over both N atoms. However, ITW was the only zeolite phase synthesized at HF/OSDA = 1.0 and 2.0 in pure-silica composition, regardless the type of TMP isomer used. Since the same result has been previously observed for the synthesis with 123TMI and 134TMI,[17] differences in the charge distribution between TMP and TMI ions may be not large enough to induce changes in the pure-silica phase selectivity.

On the other hand, when the Si/Al ratio in the synthesis mixture was fixed at 10.0, PWO and PWW were the products obtained using 134TMP and 135TMP as OSDAs at HF/OSDA =

Table 1 Representative products from zeolite syntheses using six TMP cation isomers as OSDAs at different gel Si/Al and HF/OSDA ratios in the synthesis mixture[a]

		 123TMP	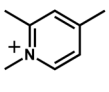 124TMP	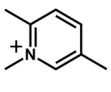 125TMP	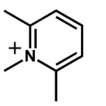 126TMP	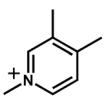 134TMP	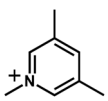 135TMP
Si/Al	HF/OSDA	Product[b]					
∞	1.0	ITW	ITW	ITW	ITW	ITW	ITW
	2.0	ITW	ITW	ITW	ITW	ITW	ITW
	3.0	ITW	Amorphous[c]	Dense	Dense	ITW	Amorphous[c]
10.0	1.0	RTH	PWO + RTH	PWO + RTH[c]	PWW + RTH	FER + RTH	PWW
	2.0	RTH	Amorphous[c]	Amorphous[c]	Amorphous[c]	PWO + amorphous[c]	PWW
	3.0	Amorphous[c]	Amorphous[c]	Amorphous[c]	Amorphous[c]	PWO[c]	Amorphous[c]

[a] The composition of the synthesis mixture is $0.5\text{R}\cdot x\text{HF}\cdot y\text{Al}_2\text{O}_3\cdot 1.0\text{SiO}_2\cdot 5.0\text{H}_2\text{O}$, where R is the OSDA, x is varied between $0.5 \leq x \leq 1.5$ and y is 0 or 0.05. All syntheses were performed under rotation (60 rpm) at 160 °C for 14 days, unless otherwise stated. OSDA abbreviations: 123TMP, 1,2,3-trimethylpyridinium; 124TMP, 1,2,4-trimethylpyridinium; 125TMP, 1,2,5-trimethylpyridinium; 126TMP, 1,2,6-trimethylpyridinium; 134TMP, 1,3,4-trimethylpyridinium; and 135TMP, 1,3,5-trimethylpyridinium. [b] The product appearing first is the major phase. [c] Product obtained after 21 days.

3.0 and 2.0, respectively. Given that 135TMP directed the synthesis of PWW even at HF/OSDA = 1.0 (Table 1), this largest TMP isomer appears to have a stronger structure-directing ability for PWW formation than the imidazolium-based OSDAs such as 134TMI.[17] We were also able to crystallize RTH from synthesis mixtures with HF/OSDA = 1.0 or 2.0 using 123TMP. These results strongly suggest that Al substitution in zeolites is the key to controlling the selectivity of crystallization in the presence of various TMP cation isomers and F^- anions. Indeed, when HF/OSDA and Si/Al were set at 0.0 and 10.0, respectively, 134TMP and 135TMP gave amorphous material even after 21 days of heating, showing the need for F^- ions during PWO and PWW crystallization.[17] On the other hand, we obtained RTH using 123TMP in hydroxide media after 14 days. However, this is not so surprising because RTH has already been reported to crystallize in the presence of many different OSDA cations under F^--free conditions.[39]

Characterization

The PXRD patterns of the representative zeolites synthesized in this study (*i.e.* 135TMP-ITW, 134TMP-PWO, 135TMP-PWW and 123TMP-RTH, all of which, except 134TMP-PWO, were obtained at HF/OSDA = 1.0) show that each zeolite is highly crystalline and there are no reflections other than those from the corresponding structures (Fig. S1†).[19] ^1H–^{13}C CP MAS NMR spectroscopy reveals that the OSDA cations employed remain intact upon their occlusion into zeolite pores (Fig. S2†). While all Al atoms in as-synthesized zeolites occupy tetrahedral framework positions, calcination at high temperatures (550–750 °C; Fig. S3†) in air to remove the occluded OSDAs resulted in the formation of a non-negligible amount of extra-framework Al

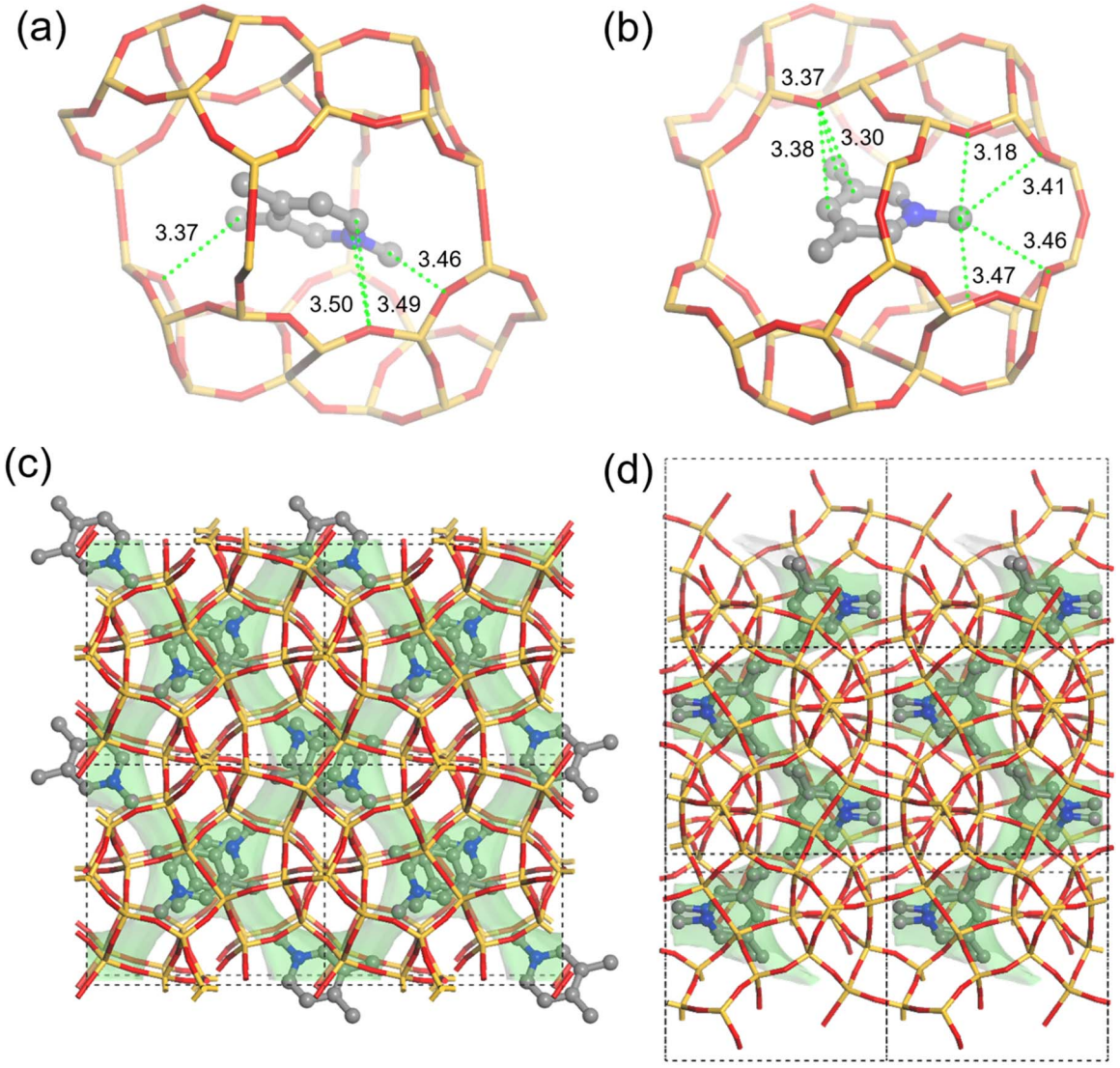

Fig. 1 (a) Octadecahedral *t-pwo* ([$4^6 5^8 9^4$]) and (b) *t-pww* ([$4^6 5^8 8^2 10^2$]) cavities of as-synthesized 134TMP-PWO and 135TMP-PWW, including the position of the OSDA. The distances between the host cages and guest molecules shorter than 3.5 Å are marked. (c) PWO and (d) PWW structures showing the refined positions of OSDAs. The PWO 9-ring and PWW 10-ring channels are marked in translucent green using accessible solvent surfaces calculated with a solvent radius of 1.4 Å. Color code: Si, yellow; O, red; C, grey; N, pale blue.

species, as evidenced by ^{27}Al MAS NMR (Fig. S4†). No significant differences in the crystal morphology were observed when TMP and TMI cations directed the synthesis of zeolites with the same framework topology. However, in the case of 135TMP-PWW and 1234TMI-PWW, the crystal width and thickness were significantly larger for the former zeolite, leading to a considerable difference (*ca.* 740 *vs.* 590 °C) in the maximum temperature of exothermic weight losses due to OSDA combustion (Fig. S3†).

Fig. 1 shows the locations and orientations of OSDA cations in as-synthesized 134TMP-PWO and 135TMP-PWW determined by the Rietveld analysis of synchrotron PXRD data (Tables S1–S5 and Fig. S5 and S6†). We did not determine the structures of as-synthesized 135TMP-ITW and 123TMP-RTH, because the location of original OSDAs in these two zeolites have already been reported.[40–42] Both 134TMP and 135TMP ions were found to reside in the intersections (*i.e.* the 18-hedral *t-pwo* ([$4^6 5^8 9^4$]) and *t-pww* ([$4^6 5^8 8^2 10^2$]) cavities, respectively) of two 9-ring channels in PWO and of 10- and 8-ring channels in PWW, with minimum distances between the TMP C and framework O atoms of 3.37 and 3.18 Å, respectively. However, the number (7 *vs.* 4) of C–O distances shorter than 3.5 Å is larger in 135TMP-PWW than in 134TMP-PWO. This can be explained by the bell shape of the *t-pww* cavity, giving a better fit to 135TMP. No signs of the presence of F^- ions in 135TMP-PWW and 134TMP-PWO were observed, despite their formation in fluoride media, in good agreement with the ^{19}F MAS NMR data in Fig. 2.

Fig. 2 shows the ^{19}F MAS NMR spectra of as-synthesized 135TMP-ITW, 134TMP-PWO, 135TMP-PWW and 123TMP-RTH. As previously reported,[43] 135TMP-ITW exhibits a sharp resonance at 40 ppm due to the F^- ions within the double 4-ring (*d4r*; 6-hedral ([46]) *t-cub*) cages, which was also observed for the other ITW zeolites synthesized here. Of particular interest is that the overall intensity of 19F resonances is exceedingly weaker in the spectra of the latter three aluminosilicate zeolites compared to pure-silica 135TMP-ITW, revealing the practical absence of F^- ions, even in their small cages like 10-hedral ([445462]) *t-tte*, 6-hedral ([4254]) *t-bru* and 8-hedral ([4454]) *t-cle* cages: very weak resonances in the range −128 to −133 ppm can be attributed to the free F^- and/or SiF_6^{2-} species within the 9- and 10-ring channels in PWO and PWW, respectively.[44–46] This indicates that in the fluoride-mediated synthesis of aluminosilicate zeolites under highly concentrated conditions, the counterbalance of OSDA cations by single framework negative charges (in the form of $[AlO_{4/2}]^-$ tetrahedra) created by Al substitution is more favorable than that by F^- ions encapsulated within small cages, probably because of the shorter cation–anion distance. Fig. 2 also shows that a resonance around 67 ppm observed for 123TMP-RTH is considerably broad compared to other zeolites, suggesting the location of F^- ions at different positions within the large *t-rth* cages.

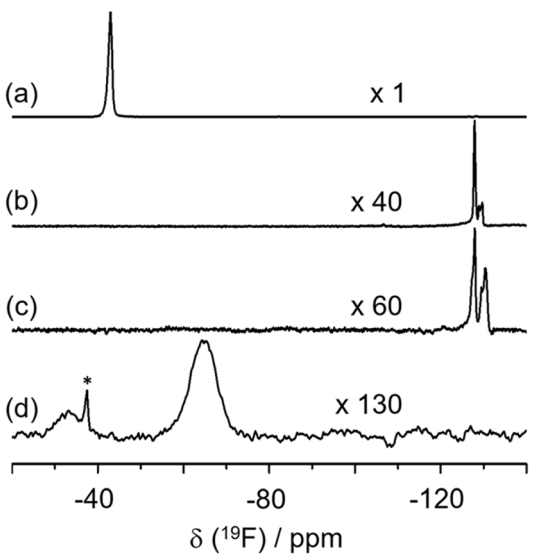

Fig. 2 ^{19}F MAS NMR spectra of as-synthesized (a) 135TMP-ITW, (b) 134TMP-PWO, (c) 135TMP-PWW and (d) 123TMP-RTH. The asterisk indicates the spinning sideband.

Elemental analysis shows that as-synthesized 134TMP-PWO, 135TMP-PWW and 123TMP-RTH have slightly higher bulk Si/Al ratios (11.5–13.8) than the ratio (10.0) of their synthesis mixtures (Tables 1 and 2). It should be noted that they possess 1.6, 2.7 and 2.2 Al atoms per unit cell that are smaller by 0.2, 1.5 and 1.6 than the numbers (1.8, 4.2 and 3.8) of OSDA cations, respectively, because all of their Al atoms are in framework positions (Fig. S4†). Therefore, charge balance requires that the positive charges of 0.2, 1.5 and 1.5 OSDAs per unit cell of 134TMP-PWO, 135TMP-PWW and 123TMP-RTH, when considering the presence of 0.1 F^- ions per unit cell in the latter zeolite, should be counterbalanced by additional negative charge centers (*i.e.* internal SiO^- groups), respectively. On the other hand, the SiO^- groups are stabilized by hydrogen bonding with water molecules and/or vicinal SiOH groups[47] to form defect sites. The chemical composition data in Table 2 reveal that as-synthesized 135TMP-PWW and 123TMP-RTH possess 0.7 and 1.3 water molecules per unit cell, which are smaller than those (1.5 both) of additional negative charge centers. Thus, we speculate that if all of their water molecules form hydrogen bonds with SiO^- groups, they should then be immobilized, giving potentially intense spinning sidebands in the ^{1}H MAS NMR spectra because of the intramolecular dipole interactions between the protons.[9] However, no such sidebands were observed in the ^{1}H MAS NMR spectra of not only 134TMP-PWO but also 135TMP-PWW and 123TMP-RTH, like the spectrum of pure-silica 135TMP-ITW (Fig. S7†). This led us to conclude, as expected, that considerable amounts of OSDA cations in our aluminosilicate zeolites must be balanced by $SiO^- \cdots$HOSi defects (Table 2).[9,16]

We applied ^{1}H DQ and TQ MAS NMR spectroscopy to ascertain the presence of $SiO^- \cdots$HOSi hydrogen bonds in as-synthesized 134TMP-PWO, 135TMP-PWW and 123TMP-RTH. Although multiple quantum transitions are quantum-mechanically forbidden for direct observation, they can be visible in a two-dimensional (2D) experiment where single quantum (SQ) chemical shifts are observable in one dimension and DQ or TQ chemical shifts in the other.[16] As shown in Fig. 3, the shoulder at a SQ chemical shift of around 9 ppm shows a ^{1}H DQ–SQ autocorrelation peak at 18.4 ppm (2 × 9.2 ppm), corresponding to the hydrogen-bonded SiOH protons at 9.2 ppm

Table 2 Physicochemical data for zeolites synthesized in this study

Sample ID	HF/OSDA[a]	Unit cell composition[b]	Si/Al	$OSDA_D/OSDA_T$[c]	Crystal shape and average size[d] (μm)	Micropore volume[e] (cm^{-3} g)
135TMP-ITW	1.0	$\|(135TMP)_{2.0}F_{2.0}(H_2O)_{0.6}\|[Si_{24}O_{48}]$	∞	0.00	Rhombic dodecahedra, 3 × 2	0.17
134TMP-PWO	3.0	$\|(134TMP)_{1.8}(H_2O)_{0.8}\|[Si_{18.4}Al_{1.6}O_{40}(OH)_{0.2}]$	11.5	0.11	Overlapped plates, 1.0 × 0.1	0.12
135TMP-PWW	1.0	$\|(135TMP)_{4.2}(H_2O)_{0.7}\|[Si_{37.3}Al_{2.7}O_{80}(OH)_{1.5}]$	13.8	0.36	Overlapped plates, 5.0 × 1.0	0.14
123TMP-RTH	1.0	$\|(123TMP)_{3.8}F_{0.1}(H_2O)_{1.3}\|[Si_{29.8}Al_{2.2}O_{64}(OH)_{1.5}]$	13.6	0.39	Rods, 15 × 2	0.24

[a] HF/OSDA ratio in the synthesis mixture that crystallized each product. [b] Determined from a combination of elemental and thermal analyses, and ^{19}F MAS NMR measurements. The water content was calculated from the endothermic weight loss by TGA/DTA up to 400 °C and OH^- (defect; see ESI eqn (4a) and (4b)) has been introduced to the zeolite framework to make the as-synthesized zeolites electrically neutral. [c] Ratio of OSDA cations compensated by $SiO^-\cdots HOSi$ defects to the total OSDA cations in each zeolite. [d] Determined by SEM. [e] Calculated from N_2 adsorption data.

with an O···O distance of 2.74 Å between SiO^- and SiOH groups,[48] is resolved for the former two zeolites. However, since no TQ signal at 27.6 ppm (3 × 9.2 ppm) was found (Fig. S8†), it is clear that 134TMP-PWO and 135TMP-PWW have two clustered SiOH groups which are hydrogen-bonded to one SiO^- group. Another interesting result is that 123TMP-RTH shows no DQ signal at 18.4 ppm, despite its higher defect concentrations (Table 2), revealing the presence of only one $SiO^-\cdots HOSi$ hydrogen bond in defect sites. The existence of $SiO^-\cdots HOSi$ defects in as-synthesized aluminosilicate zeolites obtained in hydroxide media has been previously observed.[9,49] To our knowledge, however, this has never been reported for any of the aluminosilicate zeolites synthesized in fluoride media. The ^1H DQ–SQ MAS NMR data in Fig. 3 also suggest that while the microstructure type of defects can differ according to the zeolite framework topology, they may not be primarily created by a T-atom vacancy with one SiO^- and three SiOH groups in a SiOH nest.[16] This is because the concentration of three clustered SiOH groups forming hydrogen bonds to SiO^- was below the detection limit of our NMR experiments. It is remarkable here that all of 134TMP-PWO, 135TMP-PWW and 123TMP-RTH show two pairs of DQ peaks at (9.2, 13.7) and (4.5, 13.7) ppm and (9.2, 12.0) and (2.8, 12.0) ppm, suggesting close proximities between SiOH protons hydrogen-bonded to SiO^- and the *N*- and *C*-methyl protons in TMP.

Synthesis energy calculations

To understand the origin and role of defect clusters as another important structure-directing factor in zeolite synthesis from a thermodynamic point of view, we first optimized the corresponding geometry (zeolite–OSDA) of each zeolite with various embedded TMP isomers using force fields and then calculated the E_{syn} using eqn (3a) and (3b) in the Experimental section. The lowest E_{syn} value, which corresponds to the theoretical prediction for the most stable zeolite–OSDA, has been shown to be a successful strategy,[30–32] because it can be used for any zeolite composition, even in the presence of F^- ions. For the pure-silica system, the charge of OSDA cations was counterbalanced by F^- ions within the small cavities in zeolites in order to calculate the E_{syn} values for the optimized structures (Table S6†). The results showed that ITW was the most stable pure-silica zeolite for all OSDAs, which is in excellent agreement with the experimental results (Table 1). This, once again, proves the accuracy of the synthesis energy approach in predicting the phase selectivity of pure-silica zeolite crystallization.

When zeolites have aluminosilicate composition, the characterization results revealed that, although the synthesis was performed in fluoride media, F^- ions did not get occluded in small zeolite cages (Table 2 and Fig. 1 and 2). Therefore, we first calculated their E_{syn} values in the absence of F^- ions, as well as of the experimentally observed $SiO^-\cdots HOSi$ defects, so that the positive charge of the OSDAs was only counterbalanced by $[AlO_{4/2}]^-$ tetrahedra (Table S7†). RTH was calculated to have the most favorable E_{syn} with all OSDAs when the OSDA charge was compensated only by $[AlO_{4/2}]^-$ tetrahedra. It is worth noting that the Si/Al ratio (7.0) of all these OSDA–RTH structures used in the calculations is lower than not only the ratio (10.0) of the synthesis mixture but also that (13.6) of the experimentally crystallized product. Nevertheless, the E_{syn} calculation results for aluminosilicate zeolites support the experimental observation that the charge of OSDA cations occluded is balanced by both $SiO^-\cdots HOSi$ defects and $[AlO_{4/2}]^-$ tetrahedra (Table S8†).

To include the effect of $SiO^-\cdots HOSi$ defects in our E_{syn} calculations, we derived new equations (*i.e.* eqn (3a) and (3b) in the Experimental section) and applied them to the calculations for the 135TMP and 123TMP cations embedded in FER and ITE structures, as well as in ITW, PWO, PWW and RTH with defects containing $1SiO^-$ and 1SiOH which will be designated as a 1 : 1 connectivity defect. The other structure types of defect clusters considered in this work will be explained below. The first two structures (FER and ITE) were selected because they contain the same pore system (intersecting 10- and 8-ring channels) and composite building unit (*t-cle* cage) as those of PWW and RTH, respectively.[19] The Si/Al ratio of these six zeolite structures was set to 12.3 or higher so that their Al content was always lower than that of 134TMP-PWO with the lowest Si/Al ratio (11.5) among the aluminosilicate zeolites synthesized in this study (Table 2). When the F^- ions were not included in the

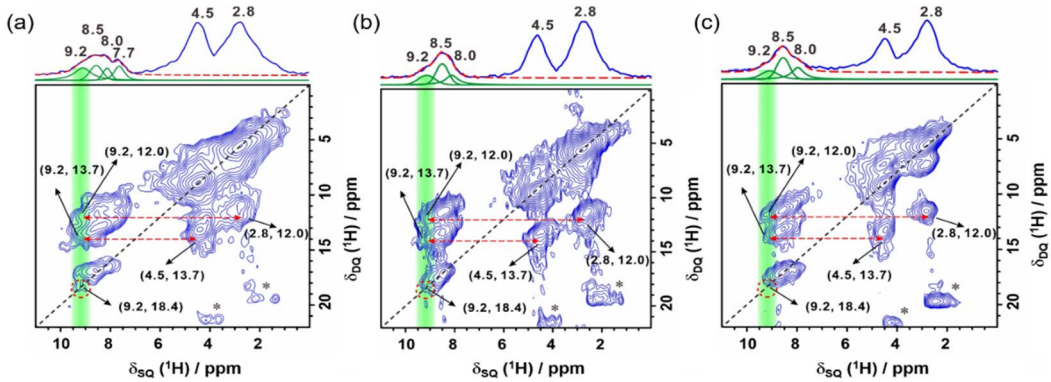

Fig. 3 ^{1}H DQ–SQ MAS NMR spectra of as-synthesized (a) 134TMP-PWO, (b) 135TMP-PWW and (c) 123TMP-RTH. The interactions between SiO^{-} and two SiOH groups and between these defects and TMP cations are indicated by red dashed circles and lines, respectively. Deconvolution of the bands centered at 8.5 ppm was done by considering ^{1}H NMR resonances of the TMP cations in D_2O. Artifacts from the rotor and probe background are marked by asterisks.

calculations, PWO and PWW, which give the lowest Si/Al ratio, were determined to be the most favorable structures in the presence of 135TMP with E_{syn} values of −0.499 and −0.472 eV per T-atom, respectively (Table S8†). This implies that they are capable of incorporating more Al atoms, in good agreement with our previous work showing that the zeolite structure with a higher Al content (or a lower Si/Al ratio) is characterized by a more favorable E_{syn} value.[30,31] However, although PWO was not experimentally synthesized with 135TMP (Table 1), the E_{syn} value of the observed PWW phase is higher by only 0.027 eV per T-atom than that of PWO. On the other hand, E_{syn} calculations for 123TMP were found to favor the formation of PWW and PWO again, unlike the experimental result giving RTH. However, since 123TMP-RTH contains only 0.1 F^{-} ions per unit cell, we calculated the E_{syn} value of 123TMP-RTH with Si/Al ∼ 14, while considering a larger number of anionic combinations to counterbalance the OSDAs (Table 2 and S9†). We note here that the addition of 2.0 F^{-} ions and 2.0 $[AlO_{4/2}]^{-}$ tetrahedra to the RTH unit cell gives a E_{syn} value of −0.627 eV per T-atom for the RTH formation (Table S9†), which is lower than that in their absence (−0.505 eV per T-atom; Table S8†) and where PWW is favored. As the amount of F^{-} ions occluded in 123TMP-RTH is negligible (Table 2), we speculate that RTH nuclei containing F^{-} ions may 'catalyse' the formation of the rest of the crystal without need of further F^{-} encapsulation.

Competition between Al substitution, F^{-} encapsulation and defect formation

Fig. 4 shows an overall view of the E_{syn} calculation results of 123TMP-RTH, 134TMP-PWO and 135TMP-PWW, using different combinations of framework Al, F^{-} ions and/or $SiO^{-}\cdots$HOSi defects for the anionic species compensating the OSDA positive charge. The E_{syn} calculation results predict that Al substitution is more favorable than F^{-} encapsulation. For RTH, the E_{syn} value (−1.043 eV per T-atom) of 123TMP-RTH with 4.0 Al atoms is far more favorable than that (−0.627 eV per T-atom) with 2.0 Al and 2.0 F^{-} ions (Table S9†). The other zeolite–OSDA pairs (*i.e.* 134TMP-PWO and 135TMP-PWW) in Fig. 4 are all showing a similar trend where Al is more readily incorporated into their structures than F^{-} ions. This supports the previous suggestion that $[AlO_{4/2}]^{-}$ tetrahedra may have stronger interactions with OSDA cations than F^{-} ions.[50]

When 123TMP-RTH has a constant number of framework Al atoms (*i.e.* 2.0 per unit cell), E_{syn} becomes more favorable by F^{-} encapsulation than by any type of $SiO^{-}\cdots$HOSi defect formation (Fig. 4 and Table S9†). Therefore, the existence of large amounts of framework defects in aluminosilicate zeolites synthesized here (Table 2) can not be explained by our energetic calculations and suggests the kinetic nature of zeolite crystallization.[13] Although thermodynamically less favorable not only than Al substitution but also F^{-} cage encapsulation, $SiO^{-}\cdots$HOSi defects are formed in the presence of Al and fluoride. We suggest that the incorporation of Al and fluoride may be limited by their restricted mobility in the gel and the stringent requirements of transport needed so that they migrate to the specific framework location in which they are close to the compensating positive charge of the OSDA. Opposite to this, $SiO^{-}\cdots$HOSi defects can be formed anywhere since they only require breaking a SiOSi linkage, without mobility constraints. We also believe that if the concentration of defects in zeolite nuclei reaches a significant level, it could then determine phase selectivity, when properly combined with the structure-directing effects of Al substitution and OSDA cations. This may be more likely in the hydroxide-mediated synthesis than in the fluoride-mediated one, given the more defective nature of the former route.[14,50]

Suggested role of fluoride in nucleation

As mentioned above, when 2.0 F^{-} ions per unit cell are incorporated into the RTH structure, the E_{syn} value of RTH (−0.627 per T-atom; Table S9†) becomes lower than the values of PWW and PWO (−0.503 and −0.505 eV per T-atom, respectively; Table S8†). Since we were not able to crystallize any aluminosilicate zeolite, as well as pure-silica ITW, in the absence of F^{-} ions, one possible hypothesis is that the nucleation of 123TMP-RTH, 134TMP-PWO and 135TMP-PWW in the aluminosilicate (Si/Al

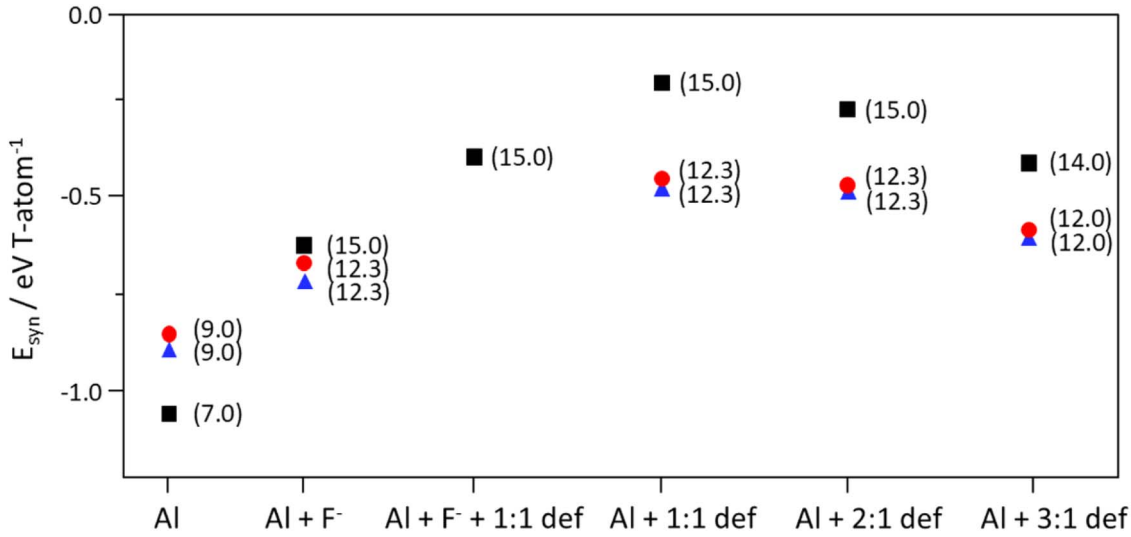

Fig. 4 E_{syn} values of zeolite–OSDA pairs with different framework Si/Al ratios and different combinations of anionic species compensating the OSDA positive charge: Al (framework Al atoms); Al + F^- (Al atoms + F^- ions); Al + F^- + def (Al atoms + F^- ions + $SiO^-\cdots HOSi$ defects); Al + def (Al atoms + $SiO^-\cdots HOSi$ defects). Three different types of defect clusters were considered: (i) 1 : 1 connectivity defects (1 : 1 def); (ii) 2 : 1 connectivity defects (2 : 1 def); and (iii) 3 : 1 vacancy defects (3 : 1 def). The pairs studied are 123TMP-RTH (black squares; Table S9†), 134TMP-PWO (blue triangles; Table S11†) and 135TMP-PWW (red circles; Table S12†). The values in the parenthesis of pair identifications are the zeolite Si/Al ratios.

= 10) synthesis mixture, as well as their crystal growth, may begin around the F^- ions, but without significant further incorporation of these anions. Thus, if the F^- ions play a catalytic role in 123TMP-RTH synthesis, this would explain why the F^- content in 134TMP-PWO and 135TMP-PWW is negligible as well (Table 2). In fact, we previously showed that all three levyne (LEV) zeolites with Si/Al = 10.7–11.0 synthesized using the same OSDA cation (*N*,*N*-dimethylpiperidinium) but at different HF/OSDA ratios (1.0–3.0) were nearly free of F^- ions.[33]

On the other hand, the E_{syn} difference (−0.689 eV per T-atom) between pure-silica 135TMP-ITW with 2.0 F^- ions or 2.0 defects per unit cell is significantly larger than that (−0.412 eV per T-atom) between aluminosilicate 123TMP-RTH with 2.0 framework Al atoms and 2.0 F^- ions and the same zeolite but with 2.0 Al atoms and 2.0 defects, highlighting the favorable interactions between fluoride anions and *d4r* units, absent in RTH,[19] of the ITW structure. It thus appears, based on our experimental and theoretical results, that once F^- ions are encapsulated within certain small cages of the growing zeolite with aluminosilicate composition, their mobility must be restricted so that further crystal growth mainly occurs around the F^- ion-containing small cages without additional F^- encapsulation.

Defects in zeolites

We calculated the E_{syn} values for 135TMP-ITW with various F^- and $SiO^-\cdots HOSi$ combinations (Table S10†). As expected, the E_{syn} value becomes less favorable when replacing F^- ions by 1 : 1 connectivity defects. This is in line with the well-known fact that the fluoride-mediated zeolite synthesis leads to the formation of far fewer internal defects than the hydroxide-mediated one, which validates our theoretical approach.[14]

Three types of defects were considered in Fig. 4, labelled as 1 : 1 def, 2 : 1 def, and 3 : 1 def, depending on the respective number (1, 2 or 3) of SiOH groups that make a hydrogen bond with the siloxy (SiO^-) group. Defects 1 : 1 and 2 : 1 belong to the class of 'connectivity defects', generated by breaking SiOSi linkages whilst '3 : 1 def' belongs to the class of 'vacancy defects' in which a Si is missing from the zeolite framework. For details on how these defects were generated, see ESI.†

The structural analysis of the calculated defects shows that in '2 : 1 def' the O···H distances between two of the SiOH groups and the SiO^- group were found to range from 1.43 to 1.52 Å, while the O···H distance for the third SiOH group exceeded 2.6 Å, indicating that only two of the SiOH groups form hydrogen bonds with the SiO^- group. Since the ^{1}H DQ–SQ MAS NMR data have shown two hydrogen-bonded SiOH per SiO^- in defect sites of 134TMP-PWO and 135TMP-PWW, it is clear that experimentally detected defects correspond to the '2 : 1 def'. For our calculated '3 : 1 def', the O···H distances between all three SiOH groups and the SiO^- group ranged from 1.47 to 1.62 Å, revealing that all three SiOH groups are hydrogen-bonded to the SiO^- group at the defect site.

For the defects, the E_{syn} calculation results in Fig. 4 suggest that the formation of 2 : 1 connectivity and 3 : 1 vacancy defects is more favorable than that of 1 : 1 defects. This is in good agreement with the ^{1}H TQ–SQ MAS NMR results of aluminosilicate PWO and PWW zeolites with a considerable amount of 2 : 1 connectivity defects (Fig. 3 and S8†). To further investigate the major defect type present in the PWO and PWW structures, we calculated the average O···O distances between SiO^- and SiOH groups in as-synthesized 134TMP-PWO, 135TMP-PWW and 123TMP-RTH zeolites, optimized by density functional theory (DFT) calculations (Table S14†). For all three zeolites, the O···O distances were calculated to range between 2.43 and 2.44 Å for 1 : 1 connectivity defects. In contrast, the 2 : 1 connectivity

defect models exhibited slightly longer O···O distances, ranging from 2.46 to 2.52 Å. These values are closer to the experimentally determined distance of 2.74 Å, derived from the ^{1}H chemical shift of 9.2 ppm (Fig. 3) using the equation by Eckert *et al.*,[48] supporting the formation of 2 : 1 connectivity defects in PWO and PWW structures.

However, the E_{syn} calculation results in Fig. 4 predict that 3 : 1 vacancy defects are energetically more favorable than the experimentally observed 2 : 1 connectivity defects. This suggests that the formation of $SiO^-\cdots HOSi$ defects and their microstructure in aluminosilicate zeolites during crystallization, at least in fluoride media, may be kinetically rather than thermodynamically controlled, which deserves further study.

Conclusions

In summary, we found that considerable amounts (11–39%) of OSDA cations in PWO, PWW and RTH zeolites with framework Si/Al ratios of 11.5–13.8 synthesized using different TMP cation isomers in concentrated fluoride media are counterbalanced by internal $SiO^-\cdots HOSi$ defects, unlike observed for pure-silica ITW zeolite whose OSDA charge is fully compensated by the fluoride anions occluded in double 4-ring units. The practical absence of F^- ions in these aluminosilicate zeolites suggests their role as a 'catalyst' in both nucleation and crystal growth processes rather than as a structure-directing agent. Experimental and theoretical analysis shows that zeolite phase selectivity for a given TMP cation in concentrated fluoride media is altered by the type and concentration of negative charge centers, most notably of framework $[AlO_{4/2}]^-$ tetrahedra and $SiO^-\cdots HOSi$ defects, although E_{syn} calculations predict that the energetic preference for zeolite–OSDA pairs studied is in the order of defect formation < F^- encapsulation < Al substitution. The E_{syn} calculation results suggest that the 3 : 1 vacancy defect is more stable than the 2 : 1 connectivity one. However, the experimental ^{1}H MAS NMR data indicate that the latter defect is predominant in PWO and PWW structures. At least, the E_{syn} calculation results agree with the experimental results in identifying the 1 : 1 connectivity defect as the least stable, consistent with their absence in these zeolites. According to these findings, pure-silica zeolites cannot be obtained from aluminosilicate mixtures, which aligns with the well-known fact that natural zeolites are aluminosilicates but not silicates. The results also suggest that defect formation may be entropically favored due to the limited mobility of framework Al atoms and encapsulated F^- ions, a hypothesis that warrants further experimental and theoretical investigations. We anticipate that our work will serve as a stimulus to elucidate the exact role of structural defects and the mechanism by which they affect the structure of the crystallizing aluminosilicate zeolite.

Data availability

The data supporting this article have been included as part of the ESI.† Crystallographic data for 134TMP-PWO and 135TMP-PWW has also been deposited at the CCDC under 2366700 and 2366701.

Author contributions

Kingsley Christian Kemp, Ömer F. Altundal, Donghui Jo and Weidong Huang: formal analysis, investigation, methodology. Qiang Wang and Feng Deng: methodology, funding acquisition. German Sastre: conceptualization, methodology, funding acquisition. Suk Bong Hong: conceptualization, methodology, project administration, funding acquisition. All authors co-wrote the paper, which involved writing the original draft as well as review and editing.

Conflicts of interest

There are no conflicts to declare.

Acknowledgements

This work was supported by the National Creative Research Initiative Program (2021R1A3A-3088711) through the National Research Foundation of Korea, EcoPro HN, the KRICT Institutional Research Program (KK2412-10), GVA (PROMETEO/2021/077), MCIN (Severo Ochoa), ASIC-UPV and SGAI-CSIC for the use of computational facilities, the International Partnership Program of the Chinese Academy of Sciences (314GJH2022022FN) and Hubei International Scientific and Technological Cooperation Program (2024EHA043) and Base (SH2303). We thank H. Koller (University of Münster) and M. A. Camblor (ICMM) for valuable discussion and PAL (Pohang, Korea) for beam time at beamline 2D (D. H. Moon) and 5A (H. H. Lee). PAL is supported by MSIP and POSTECH.

Notes and references

1 D. Fu and M. E. Davis, Carbon Dioxide Capture with Zeotype Materials, *Chem. Soc. Rev.*, 2022, **51**, 9340–9370.
2 E. Pérez-Botella, S. Valencia and F. Rey, Zeolites in Adsorption Processes: State of the Art and Future Prospects, *Chem. Rev.*, 2022, **122**, 17647–17695.
3 A. W. Chester, Y. F. Chu, R. M. Dessau, G. T. Kerr and C. T. Kresge, Aluminium-Independent Cation Exchange of Internal Siloxy Groups in ZSM-5 and ZSM-11, *J. Chem. Soc., Chem. Commun.*, 1985, 289–290.
4 W. R. Moser, R. W. Thompson, C.-C. Chiang and H. Tong, Silicon-Rich H-ZSM-5 Catalyzed Conversion of Aqueous Ethanol to Ethylene, *J. Catal.*, 1989, **117**, 19–32.
5 F. Vaudry, F. Di Renzo, F. Fajula and P. Schulz, Origin of the Optimum in Catalytic Activity of Zeolite Beta, *J. Chem. Soc., Faraday Trans.*, 1998, **94**, 617–621.
6 H. Ichihashi, Vapor Phase Beckmann Rearrangement over a High Silica MFI Zeolite, *Stud. Surf. Sci. Catal.*, 2003, **145**, 73–78.
7 K. Barbera, F. Bonino, S. Bordiga, T. V. W. Janssens and P. Beato, Structure–Deactivation Relationship for ZSM-5 Catalysts Governed by Framework Defects, *J. Catal.*, 2011, **280**, 196–205.
8 S. Prodinger, H. Shi, S. Eckstein, J. Z. Hu, M. V. Olarte, D. M. Camaioni, M. A. Derewinski and J. A. Lercher,

Stability of Zeolites in Aqueous Phase Reactions, *Chem. Mater.*, 2017, **29**, 7255–7262.
9 H. Koller, R. F. Lobo, S. L. Burkett and M. E. Davis, SiO^{-}⋯HOSi Hydrogen Bonds in As-Synthesized High-silica Zeolites, *J. Phys. Chem.*, 1995, **99**, 12588–12596.
10 I. C. Medeiros-Costa, E. Dib, N. Nesterenko, J.-P. Dath, J.-P. Gilson and S. Mintova, Silanol Defect Engineering and Healing in Zeolites: Opportunities to Fine-Tune Their Properties and Performances, *Chem. Soc. Rev.*, 2021, **50**, 11156–11179.
11 E. Dib, J. Grand, S. Mintova and C. Fernandez, Structure-Directing Agent Governs the Location of Silanol Defects in Zeolites, *Chem. Mater.*, 2015, **27**, 7577–7579.
12 E. Dib, J. Grand, A. Gedeon, S. Mintova and C. Fernandez, Control the position of framework defects in zeolites by changing the symmetry of organic structure directing agents, *Microporous Mesoporous Mater.*, 2021, **315**, 110899.
13 C. S. Cundy and P. A. Cox, The Hydrothermal Synthesis of Zeolites: Precursors, Intermediates and Reaction Mechanism, *Microporous Mesoporous Mater.*, 2005, **82**, 1–78.
14 M. A. Camblor, L. Villaescusa and M. J. Díaz-Cabañas, Synthesis of All-Silica and High-Silica Molecular Sieves in Fluoride Media, *Top. Catal.*, 1999, **9**, 59–76.
15 A. W. Burton, S. I. Zones and S. Elomari, The Chemistry of Phase Selectivity in the Synthesis of High-Silica Zeolites, *Curr. Opin. Colloid Interface Sci.*, 2005, **10**, 211–219.
16 G. Brunklaus, H. Koller and S. I. Zones, Defect Models of As-Made High-Silica Zeolites: Clusters of Hydrogen-Bonds and Their Interaction with the Organic Structure-Directing Agents Determined from ^{1}H Double and Triple Quantum NMR Spectroscopy, *Angew. Chem., Int. Ed.*, 2016, **55**, 14459–14463.
17 D. Jo, G. T. Park, J. Shin and S. B. Hong, A Zeolite Family Nonjointly Built from the 1,3-Stellated Cubic Building Unit, *Angew. Chem., Int. Ed.*, 2018, **57**, 2199–2203.
18 J. Shin, D. Jo and S. B. Hong, Rediscovery of the Importance of Inorganic Synthesis Parameters in the Search for New Zeolites, *Acc. Chem. Res.*, 2019, **52**, 1419–1427.
19 *Database of Zeolite Structures*, **https://www.iza-structure.org/databases/**, accessed February 2025.
20 E. W. Valyocsik, Synthesis of Zeolite ZSM-22 with a Heterocyclic Organic Compound, *US Pat.*, 4481177A, 1984.
21 W. J. Smith, J. Dewing and J. Dwyer, Zeolite Synthesis in the SiO_2-Al_2O_3-Na_2O-Pyridine-H_2O System, *J. Chem. Soc., Faraday Trans. 1*, 1989, **85**, 3623–3628.
22 S. J. Weigel, J.-C. Gabriel, E. G. Puebla, A. M. Bravo, N. J. Henson, L. M. Bull and A. K. Cheetham, Structure-Directing Effects in Zeolite Synthesis: A Single-Crystal X-Ray Diffraction, ^{29}Si MAS NMR, and Computational Study of the Competitive Formation of Siliceous Ferrierite and Dodecasil-3C (ZSM-39), *J. Am. Chem. Soc.*, 1996, **118**, 2427–2435.
23 G. Cao, M. J. Shah and S. C. Reyes, Synthesis of ITQ-12, *US Pat.*, 7837979B2, 2010.
24 L. Zhu, L. Ren, S. Zeng, C. Yang, H. Zhang, X. Meng, M. Rigutto, A. van der Made and F.-S. Xiao, High Temperature Synthesis of High Silica Zeolite Y with Good Crystallinity in the Presence of *N*-Methylpyridinium Iodide, *Chem. Commun.*, 2013, **49**, 10495–10497.
25 S. Cadars, M. Allix, D. H. Brouwer, R. Shayib, M. Suchomel, M. N. Garaga, A. Rakhmatullin, A. W. Burton, S. I. Zones, D. Massiot and B. F. Chmelka, Long- and Short-Range Constraints for the Structure Determination of Layered Silicates with Stacking Disorder, *Chem. Mater.*, 2014, **26**, 6994–7008.
26 H. Xu, Q. Wu, Y. Chu, J. Jiang, L. Zhang, S. Pan, C. Zhang, L. Zhu, F. Deng, X. Meng, S. Maurer, R. McGuire, A.-N. Parvulescu, U. Müller and F.-S. Xiao, Efficient Synthesis of Aluminosilicate RTH Zeolite with Good Catalytic Performances in NH3-SCR and MTO Reactions, *J. Mater. Chem. A*, 2018, **6**, 8705–8711.
27 Y. Luo, S. Smeets, F. Peng, A. S. Etman, Z. Wang, J. Sun and W. Yang, Synthesis and Structure Determination of Large-Pore Zeolite SCM-14, *Chem.–Eur. J.*, 2017, **23**, 16829–16834.
28 Y. Luo, S. Smeets, Z. Wang, J. Sun and W. Yang, Synthesis and Structure Determination of SCM-15: A 3D Large Pore Zeolite with Interconnected Straight 12×12×10-Ring Channels, *Chem.–Eur. J.*, 2019, **25**, 2184–2188.
29 Y. Ma, X. Tang, J. Hu, Y. Ma, W. Chen, Z. Liu, S. Han, C. Xu, Q. Wu, A. Zheng, L. Zhu, X. Meng and F.-S. Xiao, Design of a Small Organic Template for the Synthesis of Self-Pillared Pentasil Zeolite Nanosheets, *J. Am. Chem. Soc.*, 2022, **144**, 6270–6277.
30 Ö. F. Altundal, S. Leon and G. Sastre, Different Zeolite Phases Obtained with the Same Organic Structure Directing Agent in the Presence and Absence of Aluminum: The Directing Role of Aluminum in the Synthesis of Zeolites, *J. Phys. Chem. C*, 2023, **127**, 10797–10805.
31 Ö. F. Altundal and G. Sastre, The Directing Role of Aluminum in the Synthesis of PST-21 (PWO), PST-22 (PWW), and ERS-7 (ESV) Zeolites, *J. Phys. Chem. C*, 2023, **127**, 15648–15656.
32 J. Zeng, G. Sastre and S. B. Hong, Capturing Different Intermediate Phases During Zeolite Synthesis, *J. Am. Chem. Soc.*, 2024, **146**, 27468–27474.
33 J. Bae and S. B. Hong, Zeolite Synthesis by the Excess Fluoride Approach in the Presence of Piperidinium-based Structure-Directing Agents, *Microporous Mesoporous Mater.*, 2021, **327**, 11142.
34 H. M. Rietveld, A Profile Refinement Method for Nuclear and Magnetic Structures, *J. Appl. Crystallogr.*, 1969, **2**, 65–71.
35 M. Carravetta, M. Edén, X. Zhao, A. Brinkmann and M. H. Levitt, Symmetry Principles for the Design of Radiofrequency Pulse Sequences in the Nuclear Magnetic Resonance of Rotating Solids, *Chem. Phys. Lett.*, 2000, **321**, 205–215.
36 Y. Nishiyama, V. Agarwal and R. Zhang, *t*1-Noise Suppression by γ-Free Recoupling Sequences in Solid-State NMR for Structural Characterization of Fully Protonated Molecules at Fast MAS, *J. Phys. Chem. C*, 2020, **124**, 26332–26343.
37 M. Gálvez-Llompart, A. Cantín, F. Rey and G. Sastre, Computational Screening of Structure Directing Agents for

the Synthesis of Zeolites. A Simplified Model, *Z. Kristallogr.*, 2019, **234**, 451–460.

38 J. D. Gale, GULP: A Computer Program for the Symmetry-Adapted Simulation of Solids, *J. Chem. Soc., Faraday Trans.*, 1997, **93**, 629–637.

39 J. E. Schmidt, M. A. Deimund, D. Xie and M. E. Davis, Synthesis of RTH-Type Zeolites Using a Diverse Library of Imidazolium Cations, *Chem. Mater.*, 2015, **27**, 3756–3762.

40 D. Jo, J. B. Lim, T. Ryu, I.-S. Nam, M. A. Camblor and S. B. Hong, Unseeded Hydroxide-Mediated Synthesis and CO_2 Adsorption Properties of an Aluminosilicate Zeolite with the RTH Topology, *J. Mater. Chem. A*, 2015, **3**, 19322–19329.

41 X. B. Yang, M. A. Camblor, Y. Lee, H. M. Liu and D. H. Olson, Synthesis and Crystal Structure of As-Synthesized and Calcined Pure Silica Zeolite ITQ-12, *J. Am. Chem. Soc.*, 2004, **126**, 10403–10409.

42 B. Marler, U. Werthmann and H. Gies, Synthesis and Structure of Pure Silica-RUB-10 (Structure Type: RUT) Obtained with Pyrrolidine as the Structure Directing Agent, *Microporous Mesoporous Mater.*, 2001, **43**, 329–340.

43 P. A. Barrett, T. Boix, M. Puche, D. H. Olson, E. Jordan, H. Koller and M. A. Camblor, ITQ-12: A New Microporous Silica Polymorph and its Potential for Light Hydrocarbon Separations, *Chem. Commun.*, 2003, 2114–2115.

44 H. Koller, A. Wölker, L. A. Villaescusa, M. J. Díaz-Cabañas, S. Valencia and M. A. Camblor, Five-coordinate silicon in high-silica zeolites, *J. Am. Chem. Soc.*, 1999, **121**, 3368–3376.

45 S. I. Zones, R. J. Darton, R. Morris and S.-J. Hwang, Studies on the Role of Fluoride Ion *vs.* Reaction Concentration in Zeolite Synthesis, *J. Phys. Chem. B*, 2005, **109**, 652–661.

46 R. M. Shayib, N. C. George, R. Seshadri, A. W. Burton, S. I. Zones and B. F. Chmelka, Structure-Directing Roles and Interactions of Fluoride and Organocations with Siliceous Zeolite Frameworks, *J. Am. Chem. Soc.*, 2011, **133**, 18728–18741.

47 M. Wiebcke, Structural Links between Zeolite-Type and Clathrate Hydrate-Type Materials, *J. Chem. Soc., Chem. Commun.*, 1991, **2**, 1507–1508.

48 H. Eckert, J. P. Yesinowski, L. A. Silver and E. M. Stolper, Water in Silicate Glasses: Quantitation and Structural Studies by Proton Solid Echo and Magic Angle Spinning NMR Methods, *J. Phys. Chem.*, 1988, **92**, 2055–2064.

49 C. Schroeder, S. I. Zones, M. R. Hansen and H. Koller, Hydrogen Bonds Dominate Brønsted Acid Sites in Zeolite SSZ-42: A Classification of Their Diversity, *Angew. Chem., Int. Ed.*, 2022, **61**, e202109313.

50 M. A. Camblor, A. Corma and S. Valencia, Synthesis in Fluoride Media and Characterisation of Aluminosilicate Zeolite Beta, *J. Mater. Chem.*, 1998, **8**, 2137–2145.